Quadrupole and hexadecapole couplings for ^{127}I in Li^{127}I

Jørn Thyssen
Department of Chemistry, University of Auckland, Private Bag 92019, Auckland, New Zealand and Department of Chemistry, University of Southern Denmark, Campusvej 55, DK-5230 Odense M, Denmark

Peter Schwerdtfeger*
Department of Chemistry, University of Auckland, Private Bag 92019, Auckland, New Zealand

Michael Bender
Department of Physics and Astronomy, University of Tennessee, Knoxville, Tennessee 37996; Department of Physics and Astronomy, University of North Carolina, Chapel Hill, North Carolina 27599; and Physics Division, Oak Ridge National Laboratory, P.O. Box 2008, Oak Ridge, Tennessee 37831

Witold Nazarewicz†
Department of Physics and Astronomy, University of Tennessee, Knoxville, Tennessee 37996; Physics Division, Oak Ridge National Laboratory, P.O. Box 2008, Oak Ridge, Tennessee 37831; and Institute of Theoretical Physics, Warsaw University, ul. Hoża 69, PL-00681, Warsaw, Poland

Paul B. Semmes
Physics Department, Tennessee Technological University, Cookeville, Tennessee 38505
(Received 3 May 2000; published 8 January 2001)

The quadrupole and hexadecapole coupling constants for ^{127}I in LiI were determined from relativistic Dirac-Fock electronic structure and self-consistent nuclear structure calculations. While the calculated quadrupole coupling constant agrees with the experimental value, the predicted hexadecapole coupling constant ranges between $+6$ and $+20$ mHz, which is of opposite sign and about three orders of magnitude smaller than the value deduced from recent high resolution radio-frequency molecular beam measurements [J. Cederberg, D. Olson, A. Nelson, D. Laine, P. Zimmer, M. Welge, M. Feig, T. Höft, and N. London, J. Chem. Phys. **110**, 2431 (1999)].

DOI: 10.1103/PhysRevA.63.022505 PACS number(s): 33.15.Pw, 21.10.Ft, 21.60.−n, 27.60.+j

I. INTRODUCTION

The most accurate route to nuclear quadrupole moments is by obtaining the nuclear quadrupole coupling constants from either atomic hyperfine or microwave spectroscopy [1] of diatomic molecules and by accurate calculations of the electric field gradient using relativistic coupled cluster or multireference configuration interaction methods. This has recently been achieved for nuclides such as ^{27}Al [2], ^{39}K [3], ^{73}Ge [4], ^{85}Rb [5], ^{91}Zr [6], and ^{133}Cs [7].

Values of nuclear quadrupole moments (NQM's) for a large number of isotopes can be found in [8]. A recent update has been compiled by Pyykkö [9]; these data are displayed in Fig. 1 as a function of the atomic number Z. The trend seen in Fig. 1 is well understood and described by nuclear theory. First, the overall increase of quadrupole moments with Z and the mass number A reflects the bulk (volume) effect. (For a given deformation, the intrinsic quadrupole moment is proportional to $Z^2A^{2/3}$.) Second, the fluctuations of the NQM with Z and N (neutron number) are due to shell effects. That is, magic nuclei are spherical and the largest quadrupole deformations occur in the middle of the shell. Another elementary but important point, which needs to be emphasized in the context of Fig. 1, is that the spectroscopic NQM represents the anisotropy of nuclear charge in the *molecular reference frame* while nuclear deformations are related to *intrinsic* quadrupole moments in the body-fixed frame of a nucleus. In order to translate the measured NQM's to nuclear shape deformations, the transformation from the molecular frame to the intrinsic nuclear frame is necessary. As discussed below, in many cases this transformation is nontrivial. In particular, for weakly deformed (transitional) nuclei the concept of an intrinsic shape is not very useful. For well-deformed systems, the result strongly depends on the angular momentum of the nucleus. For instance, the NQM of a nucleus in the $I=0$ state is always zero, although this nucleus can be very well deformed intrinsically [10]. By the same token, the measured negative (positive) NQM does not have to be indicative of an oblate (prolate) intrinsic shape. The nucleus ^{127}I discussed in this paper is a nice example of such a situation.

While nuclear quadrupole deformations have been intensively studied [11], much less data are available for hexadecapole deformations. As discussed in Ref. [11], some information on hexadecapole deformations exists from Coulomb excitation studies, inelastic hadron scattering experiments, electron scattering, lifetime measurements, and hyperfine effects in muonic atoms. From shell-model arguments, it follows that for well-deformed nuclei the total intrinsic hexadecapole moment should be positive at the beginning of the

*Email address: schwerd@ccu1.auckland.ac.nz
†Email address: witek@utk.edu

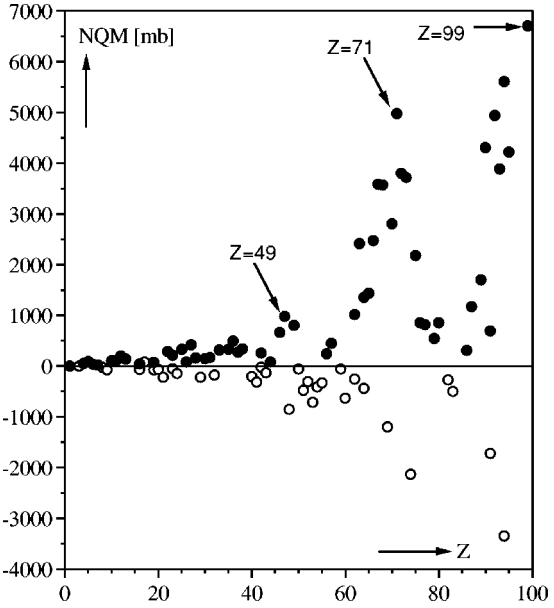

FIG. 1. Nuclear quadrupole moments for stable isotopes as functions of the nuclear charge *Z*. Experimental data are taken from [9]. Positive (negative) spectroscopic moments are indicated by filled (open) dots.

shell, and it should change sign in the middle of the shell. (See Ref. [12] for experimental systematics and discussion.)

Hexadecapole hyperfine interaction describes the coupling between the nuclear hexadecapole moment (NHM) and the electronic electric field third derivative (EFT) and is roughly $(R_N/r_e)^2$ smaller compared to the nuclear quadrupole coupling, where R_N and r_e denote the nuclear and electronic radius, respectively. This puts the hexadecapole coupling constant into the millihertz to hertz range. Because of the smallness of the hexadecapole hyperfine interaction, there is no unambiguous experimental evidence for the hexadecapolar hyperfine splitting in atoms or molecules. Based on nuclear data and theoretical calculations, the most likely candidates for the detection of the hexadecapole coupling are the elements with high quadrupole deformations such as ^{175}Lu (deformation parameters according to Ref. [13] $\beta_2 = 0.287$, $\beta_4 = -0.069$), which form simple closed-shell diatomic compounds such as LuF.

Early attempts to measure the nuclear hexadecapole coupling constant started in 1954 [14,15]. The first successful claim came in 1955 by Wang using nuclear quadrupole resonace spectroscopy (NQR) at very low temperature (0.4 °C). Wang obtained a nuclear hexadecapole coupling constant of 24 ± 5 kHz for ^{123}Sb in $SbBr_3$ [16]. In 1963, Hewitt and Williams measured NQR frequencies of ^{123}Sb in antimony metal at liquid helium temperature and obtained 13 ± 30 kHz [17]. Later in 1970, Stephenson and co-workers measured the radio-frequency spectrum of TlI using molecular beam electric resonance spectroscopy [18]. They found no evidence for nuclear hexadecapole coupling in ^{127}I above 500 Hz. The same conclusion was derived in 1973 by Hammerle and Zorn for ^{115}In in InF [19]. In 1978 Segel performed NQR measurements for ^{185,187}Re, ^{127}I, ^{209}Bi, ^{93}Nb, and ^{121,123}Sb in various solid oxo and halide compounds with no clear evidence for nuclear hexadecapole coupling [20]. A decade later in 1983, Goutou measured the ^{123}Sb hexadecapole coupling constant in $SbCl_3$ by NQR and derived 110 ± 61 kHz [21]. A single-crystal NMR experiment for ^{181}Ta in $KTaO_3$ was performed by Doering and Waugh in 1986 with no observable hexadecapole coupling above 12 kHz [22]. They also criticized Goutou's analysis, pointing out that the reported discrepancies in the fit procedure are rather due to experimental errors than due to a hexadecapole coupling. In 1991, Ni and Sears reported nuclear quadrupole resonance measurements for ^{127}I in KI claiming a hexadecapole coupling constant of 2.8 Hz [23]. Three years later, Liao and Harbison [24] found no evidence for nuclear hexadecapole coupling of the ^{127}I nucleus in CdI by NMR spectroscopy. Cederberg and co-workers [25] recently chose the less-deformed ^{127}I nucleus in molecular beam electric resonance measurements of LiI. They achieved a precision of a few hertz in the hyperfine spectrum. A careful analysis revealed that the observed data fitted best a Hamiltonian that included the hexadecapole coupling term, which resulted in a coupling constant of 15.1 ± 3.0 Hz for ^{127}I. However, they could not rule out a pseudohexadecapole effect in analogy with the electron-coupled spin–self-spin effect that is known as the pseudoquadrupole interaction [25–27].

In order to verify Cederberg *et al.*'s analysis, in this study we investigate the quadrupole and hexadecapole couplings in the ^{127}I isotope in LiI by relativistic Dirac-Hartree-Fock techniques for the electronic tensors and Skyrme Hartree-Fock and relativistic mean-field calculations for the nuclear moments. The paper is organized as follows. Section II reviews the atomic and nuclear theory of hexadecapole hyperfine interactions and moments. The computational details are given in Sec. III. The results of our calculations are discussed in Sec. IV. Finally, Sec. V contains the main conclusions of our work.

II. THEORY

A. Cartesian multipole expansion of the interaction energy

The interaction energy between two charge distributions $\varrho(\boldsymbol{r})$ and $\varrho_N(\boldsymbol{r}')$ is

$$E = \int\int d\boldsymbol{r}\, d\boldsymbol{r}' \frac{\varrho_N(\boldsymbol{r})\varrho(\boldsymbol{r}')}{|\boldsymbol{r}-\boldsymbol{r}'|} = \int d\boldsymbol{r}\left[\varrho_N(\boldsymbol{r})\int d\boldsymbol{r}' \frac{\varrho(\boldsymbol{r}')}{|\boldsymbol{r}-\boldsymbol{r}'|}\right] = \int d\boldsymbol{r}\, \varrho_N(\boldsymbol{r}) V(\boldsymbol{r}), \quad (1)$$

where the integral is over all space. In Eq. (1) $V(\boldsymbol{r})$ is the potential arising from the charge distribution $\varrho(\boldsymbol{r})$. The Cartesian multipole expansion is obtained by expanding $V(\boldsymbol{r})$ in a fourth-order Taylor series around the origin of the nucleus $\boldsymbol{r}=\boldsymbol{0}$ according to

$$V(\boldsymbol{r}) = V_0 + \left(\frac{\partial V}{d\boldsymbol{r}_\alpha}\right)_0 \boldsymbol{r}_\alpha + \frac{1}{2}\left(\frac{\partial^2 V}{\partial \boldsymbol{r}_\alpha \partial \boldsymbol{r}_\beta}\right)_0 \boldsymbol{r}_\alpha \boldsymbol{r}_\beta + \frac{1}{6}\left(\frac{\partial^3 V}{\partial \boldsymbol{r}_\alpha \partial \boldsymbol{r}_\beta \partial \boldsymbol{r}_\gamma}\right)_0 \boldsymbol{r}_\alpha \boldsymbol{r}_\beta \boldsymbol{r}_\gamma + \frac{1}{24}\left(\frac{\partial^4 V}{\partial \boldsymbol{r}_\alpha \partial \boldsymbol{r}_\beta \partial \boldsymbol{r}_\gamma \partial \boldsymbol{r}_\delta}\right)_0 \boldsymbol{r}_\alpha \boldsymbol{r}_\beta \boldsymbol{r}_\gamma \boldsymbol{r}_\delta + \cdots . \tag{2}$$

Here and in the following, greek indices run through the Cartesian coordinates (i.e., $\boldsymbol{r}_1 = x$, $\boldsymbol{r}_2 = y$, $\boldsymbol{r}_3 = z$) and the Einstein summation convention is used *for greek indices only*. Inserting Eq. (2) into Eq. (1), one obtains

$${}^{C}E = qV_0 - \mu_\alpha V_\alpha - \frac{1}{2} Q_{\alpha\beta} V_{\alpha\beta} - \frac{1}{6} R_{\alpha\beta\gamma} V_{\alpha\beta\gamma} - \frac{1}{24} H_{\alpha\beta\gamma\delta} V_{\alpha\beta\gamma\delta}, \tag{3}$$

where

$$q = \int d\boldsymbol{r}\, \varrho_N(\boldsymbol{r}), \tag{4a}$$

$$\mu_\alpha = \int d\boldsymbol{r}\, \varrho_N(\boldsymbol{r}) \boldsymbol{r}_\alpha, \tag{4b}$$

$$Q_{\alpha\beta} = \int d\boldsymbol{r}\, \varrho_N(\boldsymbol{r}) \boldsymbol{r}_\alpha \boldsymbol{r}_\beta, \tag{4c}$$

$$R_{\alpha\beta\gamma} = \int d\boldsymbol{r}\, \varrho_N(\boldsymbol{r}) \boldsymbol{r}_\alpha \boldsymbol{r}_\beta \boldsymbol{r}_\gamma, \tag{4d}$$

$$H_{\alpha\beta\gamma\delta} = \int d\boldsymbol{r}\, \varrho_N(\boldsymbol{r}) \boldsymbol{r}_\alpha \boldsymbol{r}_\beta \boldsymbol{r}_\gamma \boldsymbol{r}_\delta, \tag{4e}$$

$$V_\alpha = -\left(\frac{\partial V}{\partial \boldsymbol{r}_\alpha}\right)_0, \tag{4f}$$

$$V_{\alpha\beta} = -\left(\frac{\partial^2 V}{\partial \boldsymbol{r}_\alpha \partial \boldsymbol{r}_\beta}\right)_0, \tag{4g}$$

$$V_{\alpha\beta\gamma} = -\left(\frac{\partial^3 V}{\partial \boldsymbol{r}_\alpha \partial \boldsymbol{r}_\beta \partial \boldsymbol{r}_\gamma}\right)_0, \tag{4h}$$

$$V_{\alpha\beta\gamma\delta} = -\left(\frac{\partial^4 V}{\partial \boldsymbol{r}_\alpha \partial \boldsymbol{r}_\beta \partial \boldsymbol{r}_\gamma \partial \boldsymbol{r}_\delta}\right)_0, \tag{4i}$$

q, μ, Q, R, and H denote the nuclear monopole, dipole, quadrupole, octupole, and hexadecapole moments, respectively, and V_α, $V_{\alpha\beta}$, $V_{\alpha\beta\gamma}$, and $V_{\alpha\beta\gamma\delta}$ are the electric field, electric field gradient, electric field second derivative, and electric field third derivative, respectively. The superscript C in ${}^{C}E$ denotes the Cartesian energy expansion.

B. Spherical multipole expansion of the interaction energy

It is common to rewrite Eq. (1) using the standard multipole expansion in spherical harmonics:

$$\frac{1}{|\boldsymbol{r} - \boldsymbol{r}'|} = \sum_{\lambda=0}^{\infty} \sum_{\mu=-\lambda}^{\lambda} \frac{4\pi}{2\lambda+1} \frac{r_<^\lambda}{r_>^{\lambda+1}} Y^*_{\lambda\mu}(\hat{\boldsymbol{r}}) Y_{\lambda\mu}(\hat{\boldsymbol{r}}'), \tag{5}$$

where $r_< = \min(r, r')$ and $r_> = \max(r, r')$. Assuming $r < r'$ (i.e., assuming a pointlike nucleus) and taking only terms up to fourth order, one can rewrite Eq. (1) in the form

$${}^{S}E = \sum_{\lambda=0}^{4} \frac{4\pi}{2\lambda+1} \sum_{\mu=-\lambda}^{\lambda} \left[\int d\boldsymbol{r}\, \varrho_N(\boldsymbol{r}) Y^*_{\lambda\mu}(\hat{\boldsymbol{r}}) r^\lambda \right] \times \left[\int d\boldsymbol{r}'\, \varrho(\boldsymbol{r}') Y_{\lambda\mu}(\hat{\boldsymbol{r}}') (r')^{-\lambda-1} \right], \tag{6}$$

where the superscript S denotes the spherical multipole expansion. To compare the Cartesian energy expansion, Eq. (3), with the spherical expansion, Eq. (6), it is useful to rewrite Eq. (6) in Cartesian coordinates [28,29]:

$${}^{S}E = qV_0 - \mu_\alpha V_\alpha - \frac{1}{3} \Theta_{\alpha\beta} V_{\alpha\beta} - \frac{1}{15} \Omega_{\alpha\beta\gamma} V_{\alpha\beta\gamma} - \frac{1}{105} \Phi_{\alpha\beta\gamma\delta} V_{\alpha\beta\gamma\delta}, \tag{7a}$$

where

$$\Theta_{xx} = \int d\boldsymbol{r}\, \varrho_N(\boldsymbol{r}) r^2 P_2(\hat{x}), \tag{7b}$$

$$\Theta_{xy} = \tfrac{3}{2} \int d\boldsymbol{r}\, \varrho_N(\boldsymbol{r}) xy, \tag{7c}$$

$$\Omega_{xxx} = \int d\boldsymbol{r}\, \varrho_N(\boldsymbol{r}) r^3 P_3(\hat{x}), \tag{7d}$$

$$\Omega_{xxy} = \int d\boldsymbol{r}\, \varrho_N(\boldsymbol{r}) \left(\frac{5}{2} x^2 y - \frac{1}{2} x r^2 \right), \tag{7e}$$

$$\Omega_{xyz} = \tfrac{5}{2} \int d\boldsymbol{r}\, \varrho_N(\boldsymbol{r}) xyz, \tag{7f}$$

$$\Phi_{xxxx} = \int d\boldsymbol{r}\, \varrho_N(\boldsymbol{r}) r^4 P_4(\hat{x}), \tag{7g}$$

$$\Phi_{xxxy} = \tfrac{5}{8} \int d\boldsymbol{r}\, \varrho_N(\boldsymbol{r}) (4x^3 y - 3xy^3 - 3xyz^3), \tag{7h}$$

$$\Phi_{xxyy} = \tfrac{1}{2} \int d\boldsymbol{r}\, \varrho_N(\boldsymbol{r}) [P_4(\hat{z}) - P_4(\hat{x}) - P_4(\hat{y})], \tag{7i}$$

$$\Phi_{xxyz} = \tfrac{5}{8} \int d\boldsymbol{r}\, \varrho_N(\boldsymbol{r}) (6x^2 yz - y^3 z - yz^3). \tag{7j}$$

In the above expressions, $\hat{\boldsymbol{r}}_\alpha \equiv \boldsymbol{r}_\alpha / r$ and P_λ are the Legendre polynomials. The remaining Cartesian components in Eq. (7b) can be generated by permutation of indices. It is to be noted that in the standard derivation of Eq. (7) it is assumed that $V(\boldsymbol{r})$ fulfills the Laplace equation at the origin,

$$V_{\alpha\alpha} = -4\pi\varrho(0) = 0, \tag{8}$$

and that all the derivatives of $\varrho(\boldsymbol{r})$ vanish at $\boldsymbol{r}=\boldsymbol{0}$,

$$\left(\frac{\partial^k \varrho}{\partial \boldsymbol{r}_{\alpha_1} \partial \boldsymbol{r}_{\alpha_2} \cdots \partial \boldsymbol{r}_{\alpha_k}} \right)_0 = 0 \quad \text{for } k = 1,2,\ldots, \tag{9}$$

which guarantees that

$$V_{\alpha_1 \alpha_2 \cdots \alpha_k \alpha\alpha} = 0. \tag{10}$$

C. Transformation of the Cartesian expansion to the spherical form

It is important to realize that while the Cartesian energy expansion Eq. (3) is exact, the commonly used spherical multipole expansion Eq. (7) is not. In particular, conditions (8) and (10) cannot be met in the realistic case because the relativistic electron functions for the $s_{1/2}$ and $p_{1/2}$ states do not vanish at the origin. This implies that neither $\varrho(0)$ nor its derivatives vanish at $\boldsymbol{r}=\boldsymbol{0}$. Secondly, since the nucleus has finite size, the assumption of $r<r'$ that leads to Eq. (6) is not justified.

In order to bring the Cartesian expansion ${}^C E$ to the familiar spherical form, new traceless tensors $\tilde{V}_{\alpha\beta}$, $\tilde{V}_{\alpha\beta\gamma}$, and $\tilde{V}_{\alpha\beta\gamma\delta}$ have to be introduced. They are

$$\begin{aligned} \tilde{V}_{xx} &= V_{xx} - \frac{1}{3} V_{\alpha\alpha}, \\ \tilde{V}_{xy} &= V_{xy} \end{aligned} \tag{11}$$

(for the electric field gradient EFG),

$$\begin{aligned} \tilde{V}_{xxx} &= V_{xxx} - \frac{3}{5} V_{x\alpha\alpha}, \\ \tilde{V}_{xxy} &= V_{xxy} - \frac{1}{5} V_{y\alpha\alpha}, \\ \tilde{V}_{xyz} &= V_{xyz} \end{aligned} \tag{12}$$

(for the electric field second derivative EFS), and

$$\begin{aligned} \tilde{V}_{xxxx} &= V_{xxxx} - \frac{27}{35} V_{xx\alpha\alpha} + \frac{3}{35} V_{yy\alpha\alpha} + \frac{3}{35} V_{zz\alpha\alpha}, \\ \tilde{V}_{xxxy} &= V_{xxxy} - \frac{3}{7} V_{xy\alpha\alpha}, \\ \tilde{V}_{xxyy} &= V_{xxyy} - \frac{4}{35} V_{xx\alpha\alpha} - \frac{4}{35} V_{yy\alpha\alpha} + \frac{1}{35} V_{zz\alpha\alpha}, \\ \tilde{V}_{xxyz} &= V_{xxyz} - \frac{1}{7} V_{yz\alpha\alpha} \end{aligned} \tag{13}$$

(for the electric field third derivative EFT). The remaining Cartesian components can be generated by permutations of indices *x*, *y*, and *z*.

It is easy to check that, unlike the original electric-field tensors, the traceless tensors fulfill the conditions (8)–(10):

$$\tilde{V}_{\alpha\alpha} = 0, \tag{14}$$

$$\tilde{V}_{\alpha\beta\beta} = 0, \tag{15}$$

$$\tilde{V}_{\alpha\beta\gamma\gamma} = 0. \tag{16}$$

Moreover, when inserted into Eq. (3), the traceless tensors yield an energy expression that is formally identical to that of Eq. (7). That is,

$${}^C E(V \to \tilde{V}) = {}^S E(\tilde{V}) = {}^S E(V). \tag{17}$$

As will be discussed below in Sec. III A, the calculated values of the EFT tensor V are very large, while those obtained with the traceless EFT tensor $\tilde{V}$ are reasonably small, due to the dramatic renormalization.

Of course, the energy expressions ${}^C E$ and ${}^S\tilde{E} \equiv {}^C E(V \to \tilde{V})$ differ. This is easy to show explicitly by writing the exact Cartesian energy expansion in the following way:

$${}^C E = {}^S\tilde{E} + \sum_\lambda \Delta E^{(\lambda)}, \tag{18}$$

where $\Delta E^{(\lambda)}$ is the correction to the term of multipolarity λ in the spherical expansion due to the fact that the original potential V is not traceless.

The quadrupole correction is the well-known Poisson term [30]:

$$\Delta E^{(2)} = -\frac{1}{6} V_{\alpha\alpha} \int d\boldsymbol{r}\, \varrho_N(\boldsymbol{r}) r^2. \tag{19}$$

Since this term has a monopole character, it does not contribute to the quadrupole (or hexadecapole) splitting in first order.

Although the electric octupole splitting must be zero (nuclear states have a well-defined parity; the parity-violating effects are negligible in this context), we shall still, for the sake of completeness, derive the corresponding correction associated with the EFS:

$$\Delta E^{(3)} = -\frac{1}{10} V_{\beta\alpha\alpha} \int d\boldsymbol{r}\, \varrho_N(\boldsymbol{r}) \boldsymbol{r}_\beta r^2. \tag{20}$$

Of course, this correction vanishes since the nuclear dipole moment is zero.

For the electric field third derivative, the energy correction is

$$\Delta E^{(4)} = -\frac{1}{28} V_{\alpha\beta\gamma\gamma} \int d\boldsymbol{r}\, \varrho_N(\boldsymbol{r}) \left(\boldsymbol{r}_\alpha \boldsymbol{r}_\beta - \frac{1}{10} r^2 \delta_{\alpha\beta} \right) r^2 . \tag{21}$$

As we shall see in the following, $\Delta E^{(4)}$ can be written as a sum of monopole and quadrupole terms.

D. Limit of axial symmetry

For a linear molecule, assuming the molecular axis is the z axis, one gets

$$V_{xx} = V_{yy}, \tag{22a}$$

$$V_{xxxx} = V_{yyyy}, \tag{22b}$$

$$V_{xxzz} = V_{yyzz}, \tag{22c}$$

$$V_{xxxx} = 3V_{xxyy}. \tag{22d}$$

Due to the fact that the proton density distribution is reflection symmetric in the molecular frame, the following unique nuclear tensor components are zero:

$$\mu_\alpha = 0, \tag{23a}$$

$$R_{\alpha\beta\gamma} = 0, \tag{23b}$$

$$Q_{xy} = Q_{xz} = Q_{yz} = 0, \tag{23c}$$

$$H_{xxxy} = H_{xxxz} = H_{xxyz} = H_{xyyy} = H_{xyyz} = H_{xyzz} = H_{xzzz} = H_{yyyz} = H_{yzzz} = 0. \tag{23d}$$

In addition, since the charge density distribution is axially symmetric with respect to the molecular z axis, the following identities hold:

$$Q_{xx} = Q_{yy}, \tag{24a}$$

$$H_{xxxx} = H_{yyyy}, \tag{24b}$$

$$H_{zzxx} = H_{zzyy}, \tag{24c}$$

$$H_{xxxx} = 3H_{xxyy}. \tag{24d}$$

The resulting interaction energy can be written as

$${}^C E = qV_0 - \frac{1}{2}\Theta_{zz}\tilde{V}_{zz} - \frac{1}{24}\Phi_{zzzz}\tilde{V}_{zzzz} + \Delta E^{(2)} + \Delta E^{(4)}, \tag{25}$$

where $\Delta E^{(2)}$ is given by Eq. (19), and $\Delta E^{(4)}$, Eq. (21), can be simplified to

$$\Delta E^{(4)} = -\frac{1}{420}(2V_{zz\alpha\alpha} + V_{xx\alpha\alpha}) \int d\boldsymbol{r}\, \varrho_N(\boldsymbol{r}) r^4 \tag{26a}$$

$$-\frac{1}{84}(V_{zz\alpha\alpha} - V_{xx\alpha\alpha}) \int d\boldsymbol{r}\, \varrho_N(\boldsymbol{r})(3z^2 - r^2) r^2. \tag{26b}$$

The term (26a) has a monopole character and it does not contribute to the multipole splitting. On the other hand, the second contribution to $\Delta E^{(4)}$, Eq. (26b), has the same tensor structure as the quadrupole term in the multipole expansion. Consequently, it produces a renormalization of the quadrupole splitting.

E. The nuclear hexadecapole coupling constant

Traditionally, the nuclear hexadecapole coupling constant eHh derived from the hyperfine splitting is defined as the product of the nuclear moment $H = \Phi_{zzzz}$ and the electric-field third derivative $h = h_{zzzz} = \tilde{V}_{zzzz}$,

$$eHh = \Phi_{zzzz}\tilde{V}_{zzzz}. \tag{27}$$

The nuclear moment Φ_{zzzz} is usually given in b^2 ($1\ \mathrm{b} = 1.0 \times 10^{-28}\ \mathrm{m}^2$). As the EFT is given in a.u. (atomic units) and the nuclear hexadecapole coupling constant usually is given in hertz (Hz), a useful conversion formula is

$$eHh[\mathrm{Hz}] = \Phi_{zzzz}[\mathrm{b}^2] \times \tilde{V}_{zzzz}[\mathrm{a.u.}] \times 8.390\,741\,564. \tag{28}$$

More details can be found in Ref. [25] and we shall not repeat them here. Various conflicting definitions of h and H exist in the literature. For instance, Cederberg *et al.* define h as $h_C = h/24$. Moreover, their value of H differs from the commonly used definition of the nuclear hexadecapole moment by a factor of 4, i.e., $H_C = 4H$ (see Sec. II F below). Consequently, in order to compare our results with experimental number of Cederberg *et al.*, the following scaling has to be performed:

$$(hH)_C = \frac{1}{6} hH. \tag{29}$$

F. Nuclear multipole moments

The nuclear quadrupole ($\lambda = 2$) and hexadecapole ($\lambda = 4$) moments that enter the expression for the hyperfine splitting are the *spectroscopic* moments. Assuming the axial intrinsic density distribution, for the nuclear state characterized by angular momentum I and the projection K of the total spin on the intrinsic nuclear axis, the spectroscopic moment $Q(E\lambda)$ is given by [31]

$$Q(E\lambda) = \langle IK\lambda 0 | IK \rangle \langle II\lambda 0 | II \rangle Q_0(E\lambda), \tag{30}$$

where

$$Q_0(E\lambda) = e\left(\frac{16\pi}{2\lambda + 1} \right)^{1/2} \int \varrho_N(\boldsymbol{r}) r^\lambda Y_{\lambda 0}(\Omega) d\boldsymbol{r} \tag{31}$$

is the intrinsic multipole moment and ϱ_N is the single-particle proton density. By evaluating explicitly the Clebsch-Gordan coefficients in Eq. (30), one arrives at

$$Q(E\lambda)=f_\lambda(I,K)Q_0(E\lambda), \tag{32}$$

where

$$f_2(I,K)=\frac{3K^2-I(I+1)}{(I+1)(2I+3)}, \tag{33}$$

$$f_4(I,K)=2\frac{(2I+1)!}{(2I+5)!}[-10K^2(4K^2-1)+3(I^2+2I-5K^2) \times(I^2-5K^2-1)]. \tag{34}$$

The above expressions [Eqs. (32)–(34)] are valid in the strict limit of strong coupling [31]. In most cases, however, K is not a good quantum number and the nuclear wave function is a combination of several components having different K. The degree of K mixing strongly depends on nuclear deformation. In particular, K is not a very useful quantum number for weakly deformed nuclei where (i) the intrinsic deformed system cannot be well defined, and (ii) the Coriolis coupling is strong. In general, the nuclear wave function can be written as

$$|I\rangle=\sum_K c_K|IK\rangle. \tag{35}$$

Consequently, in the limit of the intrinsic axial shape, one obtains the following expression for the spectroscopic moment:

$$Q(E\lambda)=f_\lambda(I)Q_0(E\lambda), \tag{36}$$

where

$$f_\lambda(I)=\sum_K |c_K|^2 f_\lambda(I,K). \tag{37}$$

Note that this definition agrees with that for the quadrupole moment Q of Cederberg *et al.* but not with their definition of the hexadecapole moment H. That is, $Q_C=Q(E2)/e$ and $H_C=4Q(E4)/e$.

III. COMPUTATIONAL DETAILS

A. Electronic structure calculations

Our interest is concerned with the electric-field third-derivative tensor,

$$V^A_{\alpha\beta\gamma\delta}=V^{A,\mathrm{el}}_{\alpha\beta\gamma\delta}+V^{A,\mathrm{nuc}}_{\alpha\beta\gamma\delta}, \tag{38}$$

which, for a given nucleus A, can be expressed as a sum of the nuclear contribution,

$$V^{A,\mathrm{nuc}}_{\alpha\beta\gamma\delta}=\sum_{B\neq A}\frac{\partial^4}{\partial\alpha_A\partial\beta_A\partial\gamma_A\partial\delta_A}\frac{1}{|\boldsymbol{R}_A-\boldsymbol{R}_B|} \tag{39}$$

and the electronic contribution

$$V^{A,\mathrm{el}}_{\alpha\beta\gamma\delta}=\left\langle\Psi\left|\frac{\partial^4}{\partial\alpha_A\partial\beta_A\partial\gamma_A\partial\delta_A}\frac{1}{|\boldsymbol{r}-\boldsymbol{R}_A|}\right|\Psi\right\rangle, \tag{40}$$

where $\boldsymbol{R}_A=(x_A,y_A,z_A)$ is the position of nucleus A.

The electronic and nuclear part of the hexadecapole tensor was computed using the all-electron relativistic four-component program package DIRAC [32]. The integral program HERMIT [33] was modified to produce fourth-derivative integrals for the electronic part, and the nuclear part was calculated directly from Eq. (39). The atomic fourth-derivative integrals were transformed to the traceless form [Eq. (13)] and then contracted with the density matrix.

When constructing the traceless EFT tensor, one cannot avoid subtracting large, almost identical, integrals. As the *traceless* EFT tensor transforms as $Y_{4\mu}$, all one-center s-s, s-p, s-d, and p-d integrals can be set to zero. However, for the d-d integrals, the numerical difficulty due to cancellation cannot easily be avoided. For our relativistic four-component calculations, this is most evident in the small-component integrals, since the small-component basis set functions are generated from the large components in order to fulfill the kinetic balance condition. For example, a large-component Gaussian p function generates a small-component s and d function. Very compact (high exponent) p functions in the basis set are required to describe the $p_{1/2}$ spinor which results in a compact small-component d function. To remedy this problem, we simply decided to neglect the small-component integrals when the EFT tensor is calculated. Hence only large-component–large-component (LL) property integrals are calculated, whereas the small-component–small-component (SS) property integrals are neglected. Since the four-component operator

$$\hat{I}\tilde{V}_{zzzz}, \tag{41}$$

where $\hat{I}$ is the unity matrix, is diagonal, there are no large-component–small-component (LS) property integrals. Below, we shall estimate the error introduced by neglecting the SS property integrals.

For the Dirac-Hartree-Fock (DHF) calculations, the two-electron integrals dominate the computational effort. These integrals come in three types: LLLL, LLSS, and SSSS, where L and S denote large- and small-component basis set functions, respectively. The DHF calculations were carried out using all two-electron integrals.

The basis set used for the calculations was a well-tempered family basis set, i.e., the exponents for the basis set functions were all taken from the same master list. The exponents for iodine [34] and lithium are shown in Table I. The range of exponents used for each l quantum number was 1–28 (s), 4–28 (p), 8–27 (d), 18–27 (f) for iodine; 1–12 (s), 4–12 (p), 7–12 (d) for lithium. The experimental bond length of 2.391 924 Å [35] was used in all calculations.

B. Nuclear structure calculations

The equilibrium shapes of ^{127}I in several low lying quasiparticle states were calculated with the self-consistent mean-field theory. In order to assess the uncertainties arising

TABLE I. Exponents for family basis sets for I and Li. The exponents for iodine are taken from Ref. [34].

No.	I exponents	Li exponents
1	109066880.00000000	1950.00810000
2	23490795.00000000	439.43845000
3	5726263.50000000	103.39728000
4	1568306.70000000	25.45163800
5	478497.25000000	6.56816480
6	161092.95000000	1.78119720
7	59231.11900000	0.50891349
8	23530.84100000	0.15363426
9	9991.88790000	0.04916296
10	4487.66590000	0.01673633
11	2110.92280000	0.00608594
12	1030.64160000	0.00237500
13	518.19560000	
14	266.49834000	
15	139.40228000	
16	73.83244900	
17	39.45256600	
18	21.21128400	
19	11.45092200	
20	6.19812970	
21	3.36036180	
22	1.82356800	
23	0.99010488	
24	0.53771463	
25	0.29205998	
26	0.15863939	
27	0.08616991	
28	0.04680599	

from nuclear structure models, we have performed calculations with two different successful mean-field models, namely, the (nonrelativistic) Skyrme Hartree-Fock (HF) model and the relativistic mean-field (RMF) model. In both cases, the nucleons are described as pointlike particles moving independently in a common self-consistent field. Both models employ effective interactions specially designed for the purpose of nuclear mean-field calculations. The total binding energy is formulated in terms of an effective energy functional which depends on local densities and currents only. This links the HF and RMF models to the effective energy functional theory in the Kohn-Sham approach [36] which was originally developed for many-electron systems.

For both models there is a large variety of parametrizations of the effective interaction to be found in the literature. All of them are developed through fits to experimental nuclear data, but with different bias. Of course, the basic ground-state properties of spherical nuclei (energy, radius) are always well reproduced. Small variations appear with respect to further demands.

Our implementation of the HF model is based on the standard ansatz [37] for the effective interaction which employs a completely local energy functional. From the large pool of Skyrme interactions that are available nowadays, we have selected two typical samples of comparable (high) quality from recent fits. The parametrization SLy6 [38,39] gives a good overall description of nuclear bulk properties of spherical and deformed nuclei. The parametrization SkX [40] was fitted with a bias to a good description of single-particle properties.

In the RMF model, nucleons are described as independent Dirac particles moving in local isoscalar-scalar, isoscalar-vector, and isovector-vector mean fields usually associated with σ, ω, and ρ mesons, respectively (see Ref. [41] and references therein). As in the HF model, there exist many RMF parametrizations which differ in details. For the purpose of the present study, we chose two successful recent forces, NL-Z2 [42] and NL3 [43], which give a good description of nuclear bulk and single-particle properties throughout the chart of nuclei.

The energy functional of the effective nuclear interaction in both models is, of course, complemented by the Coulomb interaction for the protons. In the HF and RMF models, pair correlations of the nucleons are treated within the BCS scheme using a (nonrelativistic) δ pairing force (see [42] and references therein for details). We find that the soft potential energy surface of the transitional nucleus ^{127}I is sensitive to small changes in the pairing strength. To minimize the uncertainties from the pairing interaction, we have adjusted the pairing strength (separately for protons V_p and neutrons V_n) to the odd-even staggering of nuclear masses for the semimagic nuclei ^{127}Sn and ^{135}I. The values obtained are $V_n=-263$ and $V_p=-305$ for SLy6, $V_n=-212$ and $V_p=-270$ for SkX, $V_n=-385$ and $V_p=-440$ for NL3, and $V_n=-343$ and $V_p=-350$ for NL-Z2, all in units of MeV fm^3.

For both models, the mean-field equations are solved on an axially symmetric grid assuming reflection symmetry. Nuclei with odd mass number are calculated in a self-consistent blocking approximation (see [44] for details), taking into account time-odd contributions to the single-particle Hamiltonian as described in [45] for HF and [44] for RMF. This includes the core polarization effects induced by the blocked particle in a self-consistent way.

In order to relate self-consistent results to other calculations it is convenient to introduce the axial deformation parameters β_λ, which, for small deformations, are proportional to the intrinsic electric moments (31) [11]:

$$\beta_\lambda=\frac{\sqrt{(2\lambda+1)\pi}}{3ZeR_0^\lambda}Q_0(E\lambda), \tag{42}$$

where $R_0=1.2A^{1/3}$ fm.

IV. RESULTS AND DISCUSSION

A. Equilibrium deformations of ^{127}I

The proton Fermi level of ^{127}I lies in the vicinity of the $d_{5/2}$ and $g_{7/2}$ shells. The deformed Nilsson orbitals that appear around $Z=53$ are the low-K [420]1/2 and [422]3/2 (prolate) and high-K [402]5/2 and [404]7/2 (oblate) states. According to the calculations of Ref. [46], all four of these

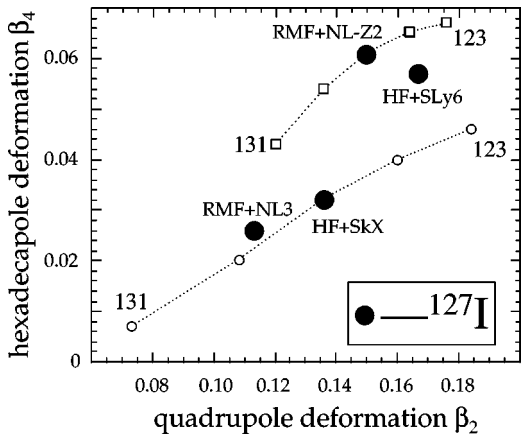

FIG. 2. Quadrupole and hexadecapole proton equilibrium deformations calculated for ^{123,125,127,129,131}I in the HF + SkX and RMF + NL-Z2 models. The deformations for ^{127}I predicted in the HF + SLy6 and RMF + NL3 models are also shown.

one-quasiproton states appear very close in energy. Experimentally, the ground state of ^{127}I is a $5/2^+$ state, and there is an excited $7/2^+$ level at 58 keV. Built on both levels (associated with proton $d_{5/2}$ and $g_{7/2}$ excitations, respectively) there are decoupled quasirotational bands [47]. At higher excitation energy (around 1.2 MeV), there appear rotational bands built upon the $g_{9/2}$ ([404]9/2) and $h_{11/2}$ intruder orbitals.

Having only three valence protons and eight valence neutron holes, ^{127}I is a weakly deformed transitional nucleus. Recently, ^{127}I received considerable interest because of its applications in solar-neutrino detectors [48]. In several theoretical papers, the structure of ^{127}I was investigated, especially in the context of β decay, Gamow-Teller strength, and neutrino-nucleus scattering [49–51]. All these works employed the shell-model framework in a limited configuration space. In particular, in Ref. [50] predictions were made for the ground-state quadrupole moment of ^{127}I using the quadrupole effective charges appropriate to the $A\approx 130$ mass region (i.e., $e_p=1.5e$ and $e_n=0.5e$). Unfortunately, since the hexadecapole effective charges are not known, one is bound to use the no-core mean-field approach, and this is the strategy that we adopted in the present study.

According to our configuration-constrained axial mean-field calculations, the four Nilsson orbitals [420]1/2, [422]3/2, [402]5/2, and [404]7/2 appear close in energy. The quadrupole and hexadecapole deformations for the [422]3/2 Nilsson level, predicted to be the best deformed in our calculations, are shown in Fig. 2. It is seen that the quadrupole deformation ranges from $\beta_2=0.17$ (HF + SLy6) to $\beta_2=0.11$ (RMF + NL3), and the hexadecapole deformation β_4 varies between 0.057 (HF + SLy6) and 0.026 (RMF + NL3). The shapes of the neighboring iodine isotopes are fairly similar (see Fig. 2). The [420]1/2 one-quasiparticle state is calculated to be slightly less deformed (e.g., $\beta_2=0.14$ in HF + SLy6) but its hexadecapole deformation is still positive. Both the [402]5/2 and [404]7/2 one-quasiparticle states are predicted to be oblate. For instance, the calculated proton deformations for the [402]5/2 state are $\beta_2=-0.14$, $\beta_4=0.014$ in the HF + SkX model and $\beta_2=-0.14$, $\beta_4=0.009$ in HF + SLy6. In the RMF calculations, quadrupole deformations are lower ($-0.09<\beta_2<-0.05$) and hexadecapole deformations are close to zero.

TABLE II. Factors [Eq. (33) and Eq. (34)] relating intrinsic multipole moments to spectroscopic moments for $I=5/2$. Note that f_2 is negative for $K=1/2$ and 3/2 and f_4 changes sign when going from $K=1/2$ to $K=3/2$.

K	$f_2(5/2,K)$	$f_4(5/2,K)$
1/2	−0.29	0.048
3/2	−0.07	−0.072
5/2	0.36	0.024

The predicted closeness of prolate and oblate structures and fairly small equilibrium deformations suggest that triaxiality could play a role in the ground state of ^{127}I and that dynamical correlations can influence the predicted multipole moments. One should bear this in mind when estimating nuclear quadrupole and hexadecapole moments in this nucleus using the static mean-field approach.

According to Eq. (36), the measured spectroscopic moment is proportional, but not equal, to the intrinsic moment. The proportionality coefficient depends on the angular momentum of nuclear state and its K distribution. In the limit of good K, one can use expressions (32)–(34). For the $I=5/2$ state, the corresponding values of $f_\lambda(I,K)$ are displayed in Table II. One can see that f_2 is negative for $K=1/2$ and 3/2, and that f_4 changes sign between $K=1/2$ and 3/2. Consequently, the actual sign of the spectroscopic moment not only depends on the nuclear shape (i.e., the sign of the intrinsic moment) but can also depend rather strongly on the degree of K mixing.

Due to the relatively small deformation, one expects strong Coriolis coupling, which should give rise to rotationally aligned configurations. Indeed, the fact that the ground state of ^{127}I has $I^\pi=5/2^+$, that there appears a low lying $I^\pi=7/2^+$ level, and that there are decoupled quasirotational bands built upon them, all suggest that one is close to the limit of rotational alignment. In this limit, the expansion coefficients c_K in Eq. (35) are given by the rotation matrices $d^j_{jK}(\pi/2)$ with $j=I$ (see, e.g., the discussion in Ref. [52]), and the resulting values of $f_2(5/2)$ and $f_4(5/2)$ are –0.18 and 0.009, respectively. This yields the nuclear quadrupole moment in the range $-0.44<Q(E2)<-0.29$ b, assuming prolate deformations calculated with different mean-field models. According to recent work [53], the nuclear quadrupole moment of ^{127}I is –0.69(3) b, i.e., it is significantly larger in magnitude. For the oblate shapes, employing the strong coupling expression, one obtains $-0.74<Q(E2)<-0.47$ b. Although this result is closer to the data, the absence of a strongly coupled ground-state band indicates that the $I^\pi=5/2^+$ ground state of ^{127}I does not have a high K character.

For the hexadecapole moments, in the limit of rotational alignment, one obtains a dramatic reduction of the intrinsic value due to a very small $f_4(5/2)$ factor. For the prolate configurations, the resulting values of the nuclear hexadecapole moment lie in the range $6\times10^{-4}<Q(E4)<2$

TABLE III. Calculated and observed quadrupole and magnetic moments, and $B(E2)$ values for the low lying states in ^{127}I. The measured magnetic moment for the $3/2^+$ state at 203 keV is 0.97(0.07) n.m.; the calculated value for the lowest $3/2^+$ state at prolate deformations is 0.8 n.m. The $B(E2)$ rates are given in Weisskopf units [1 W.u.$=(1.2)^2/(4\pi)(3/5)^2A^{4/3}\ e^2\mathrm{fm}^4$]. (The experimental data are taken from Refs. [47,53].)

β_2	β_4	$Q_2(5/2)$ (e b)	$\mu(5/2)$ (n.m.)	$Q_2(7/2)$ (e b)	$\mu(7/2)$ (n.m.)	$B(9/2\rightarrow5/2)$ (W.u.)	$B(11/2\rightarrow7/2)$ (W.u.)
0.17	0.049	−0.60	3.3	−0.60	2.0	2.3	41
0.14	0.028	−0.40	3.5	−0.51	2.1	29	2.7
−0.14	0.009	−0.64	3.3	−0.77	2.5	9.4	10.5
Expt.		−0.69	2.8	−0.71	2.5	3.6(5)	40(8)

$\times10^{-3}$ b^2, i.e., they are very small and positive. Assuming oblate shapes and the strong coupling approximation, one obtains $Q(E4)\approx0$.

B. Particle-plus-rotor calculations and *K* mixing

Since the Coriolis mixing plays such an important role for the reliable prediction of nuclear moments in ^{127}I, we decided to perform particle-plus-rotor model (PRM) calculations. In this model [31], the total angular momentum of an odd-mass nucleus is written as a sum of the single-particle angular momentum of an odd nucleon and that of the deformed core. Since the PRM Hamiltonian is explicitly constructed in the intrinsic (rotating) reference frame, the Coriolis mixing is properly accounted for.

Our PRM calculations were performed using the formalism of Ref. [54] but with the Woods-Saxon potential for the deformed mean field [55]. A number of calculations were made with deformations motivated by the HF and RMF results, and qualitatively similar features were found for all the prolate shapes considered. The proton Fermi level and pairing gap were obtained from a standard BCS calculation. The moment of inertia was estimated from Grodzins' rule [56], and for $\beta_2=0.17$ this resulted in a core 2^+ energy of 0.522 MeV, which is rather close to the average 2^+ energy of the neighboring even-even nuclei ^{126}Te and ^{128}Xe (0.555 MeV). The spin g factor for the odd proton was taken as 70% of the free value, and the core g_R value was estimated as Z/A.

As in the self-consistent calculations, the Nilsson states that are closest to the Fermi level at $\beta_2\approx0.17$ are the [420]1/2, [431]1/2, and [422]3/2 orbitals, although a sufficiently large number of Nilsson states are included to ensure numerical convergence. Rotational mixing between low K states is usually very strong, and consequently the low energy states in ^{127}I are expected to be significantly distorted from the simple strong coupled band patterns.

The PRM calculations for prolate shape reproduce the general features of rotational bands observed in ^{127}I. Furthermore, some electromagnetic properties are compared in Table III, and these are very well described, even though the calculated states are rather mixed. The large admixture of components with $K<I$ accounts for the negative observed (spectroscopic) quadrupole moment (cf. Table II and the discussion above). The predicted hexadecapole moments are small and positive, 6×10^{-3} b^2 at $\beta_2=0.17$ and 2×10^{-3} b^2 at $\beta_2=0.14$. This is consistent with the simple estimates shown above.

It is interesting to note that the calculations performed for the oblate shape also give reasonable results for the electromagnetic moments (see Table III). The hexadecapole moment is positive and very small, 6×10^{-4} b^2. However, since at oblate deformations the $K=5/2$ and 7/2 Nilsson orbitals are rather pure high K states, calculations yield a clear strong coupled band pattern built on these levels, and this disagrees strongly with experimental data.

C. The hexadecapole coupling constant

The calculated electric field derivatives are given in Table IV. These, combined with nuclear multipole moments, yield the nuclear multipole coupling constants given in Table V.

For the quadrupole coupling, the calculated results agree reasonably well with the experimentally obtained value. A more precise calculation of the NQCC was not the main purpose of this work and would require the inclusion of electron correlation effects, a better basis set, and the inclusion of zero-point vibrational effects. It is unlikely that these effects are larger than 10%–15% (±25 MHz), which we give as the uncertainty. We note that the results listed in Table IV show that neglecting the SS part has only a very small effect (approx. 2%) on the property matrix.

The correction to the quadrupole constant originating from the hexadecapole term, Eq. (26b), can easily be estimated by noting that in the liquid-drop model

TABLE IV. Electric-field derivatives along the molecular axis for iodine in LiI calculated at the DHF level. All values are given in atomic units.

	Integrals[a]	Electronic contribution	Nuclear contribution	Total
EFG ($\tilde{V}_{zz}$)	LL + SS	0.9801	0.0547	1.0450
EFG ($\tilde{V}_{zz}$)	LL	0.9553	0.0547	1.0203
EFT ($\tilde{V}_{zzzz}$)	LL	7.2358	0.0382	7.2740

[a]The integrals used in the calculation of the property integrals. The actual DHF calculations were all carried out using all (LLLL, LLSS, and SSSS) integrals.

TABLE V. Calculated and experimental nuclear multipole coupling constants. The uncertainty given is in the units of the last significant digit.

	Experimental [25]	Calculated
NQCC (MHz)	−194.351212 (17)	−174[a]
		−169[b]
		−147[c]
NHCC (Hz)	−15.1 (30)	+0.060[d]
		+0.020[e]

[a]Calculated using a nuclear quadrupole moment of $Q(E2)=-0.71$ b (Ref. [9]).
[b]Calculated using a nuclear quadrupole moment of $Q(E2)=-0.69$ b (Ref. [53]).
[c]Calculated using a theoretical nuclear quadrupole moment of $Q(E2)=-0.60$ b.
[d]Calculated using a nuclear hexadecapole moment of $Q(E4)=+0.006$ b^2 (see Sec. II F).
[e]Calculated using a nuclear hexadecapole moment of $Q(E4)=+0.002$ b^2 (see Sec. II F).

$$\int d\boldsymbol{r}\,\varrho_N(\boldsymbol{r})(3z^2-r^2)r^2\approx Q(E2)R^2. \tag{43}$$

By taking $Q(E2)=-0.69$ b, $R=5$ fm, and the calculated value of $V_{zz\alpha\alpha}-V_{xx\alpha\alpha}=1.45\times10^5$ a.u., the resulting correction becomes

$$\delta(qQ)=-\frac{1}{21}Q(E2)R^2(V_{zz\alpha\alpha}-V_{xx\alpha\alpha})=-10.0 \text{ kHz}, \tag{44}$$

i.e., its magnitude is about four orders smaller compared to the experimental value of the NQCC (−194 MHz). This term has been neglected so far in all electronic field gradient calculations and clearly limits the precision to which nuclear quadrupole moments can be determined from nuclear quadrupole coupling constants. We also note that the calculation of $(V_{zz\alpha\alpha}-V_{xx\alpha\alpha})$ requires all one-center *s-p*, *p-p*, *s-d*, and *p-d* integrals.

For the EFT we cannot estimate the effect of neglecting SS integrals in the property matrix due to the numerical problems described above. However, as the effect is 2% for the EFG, we estimate that the error is not much larger for the EFT. As for the EFG, a more precise calculation should include correlation and zero-point vibrational effects and use better basis sets. Again, we estimate these effects are of the same size as for the EFG. Thus, the total uncertainty is estimated to be smaller than 25%. Our calculations predict the nuclear hexadecapole coupling constant to be in the range of +20 to +60 mHz whereas the experimental range is −18 to −12 Hz. Hence the calculated and experimental nuclear hexadecapole coupling constants differ by three orders of magnitude and the sign.

V. CONCLUSIONS

The main conclusions of our nuclear and electronic structure calculations can be summarized as follows.

(1) The low energy experimental data for ^{127}I (band structures, electromagnetic transitions, and moments) are consistent with a slightly deformed prolate shape ($\beta_2\approx0.17$) and small, but positive, hexadecapole deformation. The resulting quadrupole moment is negative and the hexadecapole moment is positive.

(2) The calculated quadrupole and hexadecapole moments and their signs are sensitive to the *K* mixing resulting from the Coriolis coupling. Moreover, since ^{127}I is a transitional nucleus, triaxial degrees of freedom may play a role; the reliable estimate of the full hexadecapole tensor $Q(E4,\mu)$ would require a theory that goes beyond the static mean-field approximation. However, we do not expect the resulting corrections to affect the calculated multipole moments significantly.

(3) The calculated hexadecapole coupling constant for ^{127}I is in the range of tens of millihertz and about three orders of magnitude smaller than the experimentally determined value. In addition, it is of opposite sign from the extracted experimental value. It is therefore likely that the experimental splitting originates from part of the second-order quadrupole (''pseudohexadecapole'') interaction [57] rather than from the hexadecapole interaction (see the discussion in Ref. [25]). A rough estimate using $(eqQ)^2/\Delta E$ for LiI shows that for rotational transitions this term can easily be in the hertz to kilohertz range.

(4) The transitional nucleus ^{127}I is perhaps not the best choice for an experimental search for a hexadecapole hyperfine splitting. Much better candidates are the well-deformed rare-earth nuclei [13] or actinides [58] with predicted large hexadecapole moments such as ^{175}Lu. Moreover, for these nuclei the static description and strong coupling are expected to work very well, thus minimizing the nuclear uncertainty.

ACKNOWLEDGMENTS

This research was supported by the U.S. Department of Energy under Contract Nos. DE-FG02-96ER40963 (University of Tennessee), DE-FG02-97ER41019 (University of North Carolina), DE-AC05-00OR22725 with UT-Battelle, LLC (Oak Ridge National Laboratory), DE-FG02-92ER40694 (Tennessee Technological University), the Marsden Fund Wellington, the Royal Society of New Zealand, and the Auckland University Research Committee. We are very grateful to Professor Jim Cederberg for valuable discussions and comments.

[1] N. F. Ramsey, *Nuclear Moments* (Wiley, New York, 1953).
[2] V. Kellö, A. J. Sadlej, P. Pyykkö, D. Sundholm, and M. Tokman, Chem. Phys. Lett. **302**, 414 (1999).
[3] V. Kellö and A. J. Sadlej, Chem. Phys. Lett. **292**, 403 (1998).
[4] V. Kellö and A. J. Sadlej, Mol. Phys. **96**, 275 (1998).
[5] V. Kellö and A. J. Sadlej, Phys. Rev. A **60**, 3575 (1999).
[6] V. Kellö, P. Pyykkö, A. J. Sadlej, P. Schwerdtfeger, and J. Thyssen, Chem. Phys. Lett. **318**, 222 (2000).

[7] M. Pernpointer, P. Schwerdtfeger, and B. A. Hess, J. Chem. Phys. **108**, 6739 (1998).
[8] P. Rhagavan, At. Data Nucl. Data Tables **42**, 189 (1989).
[9] P. Pyykkö, Report No. HUKI 1-92, Helsinki, 1992, available from http://www.shef.ac.uk/uni/academic/A-C/chem/web-elements/
[10] P. Jacquinot and R. Klapisch, Rep. Prog. Phys. **42**, 773 (1979).
[11] W. Nazarewicz and I. Ragnarsson, in *Handbook of Nuclear Properties*, edited by D. Poenaru and W. Greiner (Clarendon, Oxford, 1996), p. 80.
[12] J. Jänecke, Phys. Lett. **103B**, 1 (1981).
[13] P. Möller, J. R. Nix, W. D. Myers, and W. J. Swiatecki, At. Data Nucl. Data Tables **59**, 185 (1995).
[14] V. Jaccarino, J. G. King, R. A. Satten, and H. H. Stroke, Phys. Rev. **87**, 1798 (1954).
[15] P. Kusch and T. G. Eck, Phys. Rev. **87**, 1799 (1954).
[16] T.-C. Wang, Phys. Rev. **99**, 566 (1955).
[17] R. R. Hewitt and B. F. Williams, Phys. Rev. **129**, 1188 (1963).
[18] D. A. Stephenson, J. T. Dickinson, and J. C. Zorn, J. Chem. Phys. **53**, 1529 (1970).
[19] R. H. Hammerle and J. C. Zorn, Phys. Rev. C **7**, 1591 (1973).
[20] S. L. Segel, J. Chem. Phys. **69**, 2434 (1978).
[21] H. Goutou, J. Magn. Reson. **54**, 36 (1983).
[22] E. B. Doering and J. S. Waugh, J. Chem. Phys. **85**, 1753 (1986).
[23] Q. W. Ni and R. E. J. Sears, J. Chem. Phys. **95**, 4796 (1991).
[24] M.-Y. Liao and G. S. Harbison, J. Chem. Phys. **100**, 1895 (1994).
[25] J. Cederberg, D. Olson, A. Nelson, D. Laine, P. Zimmer, M. Welge, M. Feig, T. Höft, and N. London, J. Chem. Phys. **110**, 2431 (1999).
[26] P. Pyykkö and J. Linderberg, Chem. Phys. Lett. **5**, 34 (1970).
[27] H. B. Jansen and P. Pyykkö, in *Methods and Structure of Quantum Science*, edited by J.-L. Calais *et al.* (Plenum Press, New York, 1976), p. 409.
[28] A. D. McLean and M. Yoshimine, J. Chem. Phys. **47**, 1927 (1967).
[29] D. L. Andrews and W. A. Ghoul, Phys. Rev. A **25**, 2647 (1982), and references therein.
[30] M. Pernpointner, P. Schwerdtfeger, and B. A. Hess, Int. J. Quantum Chem. **76**, 371 (2000).
[31] A. Bohr and B. Mottelson, *Nuclear Structure* (W. A. Benjamin, New York, 1975), Vol. 2.
[32] T. Saue, T. Enevoldsen, T. Helgaker, H. J. Aa. Jensen, J. Laerdahl, K. Ruud, J. Thyssen, and L. Visscher, Computer code DIRAC, release 3.1 (http://dirac.chem.sdu.dk), 1998.
[33] T. Helgaker, H. J. Aa. Jensen, P. Jørgensen, J. Olsen, K. Ruud, H. Ågren, T. Andersen, K. L. Bak, V. Bakken, O. Christiansen, P. Dahle, E. K. Dalskov, T. Enevoldsen, B. Fernandez, H. Heiberg, H. Hettema, D. Jonsson, S. Kirpekar, R. Kobayashi, H. Koch, K. V. Mikkelsen, P. Norman, M. J. Packer, T. Saue, P. R. Taylor, and O. Vahtras, Computer code DALTON, release 1.0, 1997 (http://www.kjemi.uio.no/software/dalton/dalton.html).
[34] S. Huzinaga and M. Klobukowski, Chem. Phys. Lett. **212**, 260 (1993).
[35] K. P. Huber and G. Herzberg, *Molecular Spectra and Molecular Structure* (Van Nostrand, New York, 1979), Vol. VI.
[36] W. Kohn and L. J. Sham, Phys. Rev. **140**, A1133 (1965).
[37] P. Quentin and H. Flocard, Annu. Rev. Nucl. Part. Sci. **28**, 523 (1978).
[38] E. Chabanat, Ph.D. thesis, Université Claude Bernard Lyon-1, 1995.
[39] E. Chabanat, P. Bonche, P. Haensel, J. Meyer, and R. Schaeffer, Nucl. Phys. A **635**, 231 (1998).
[40] B. A. Brown, Phys. Rev. C **58**, 220 (1998).
[41] P.-G. Reinhard, Rep. Prog. Phys. **52**, 439 (1989).
[42] M. Bender, K. Rutz, P.-G. Reinhard, J. A. Maruhn, and W. Greiner, Phys. Rev. C **60**, 034304 (1999).
[43] G. Lalazissis, J. König, and P. Ring, Phys. Rev. C **55**, 540 (1997).
[44] K. Rutz, M. Bender, J. A. Maruhn, P.-G. Reinhard, and W. Greiner, Nucl. Phys. A **634**, 67 (1998).
[45] J. Dobaczewski and J. Dudek, Phys. Rev. C **52**, 1827 (1995).
[46] Y. Liang, D. B. Fossan, J. R. Hughes, D. R. LaFosse, R. Ma, E. S. Paul, P. Vaska, M. P. Waring, N. Xu, J. Y. Zhang, and W. Nazarewicz, in *Proceedings of the International Conference on High Spin Physics and Gamma-Soft Nuclei, Pittsburgh 1990*, edited by J. Saladin, R. Sorensen, and C. Vincent (World Scientific, Singapore, 1991), p. 308.
[47] R. Firestone and V. Shirley, *Table of Isotopes* (Wiley, New York, 1996), Vol. I.
[48] W. Haxton, Phys. Rev. Lett. **60**, 768 (1988).
[49] J. Engel, S. Pittel, and P. Vogel, Phys. Rev. C **50**, 1702 (1994).
[50] M. Ressell and D. Dean, Phys. Rev. C **56**, 535 (1997).
[51] J. Toivanen and J. Suhonen, Phys. Rev. C **57**, 1237 (1998).
[52] G. D. Dracoulis, T. Lonnroth, S. Vajda, O. C. Kistner, M. H. Rafailovich, E. Dafni, and G. Schatz, Phys. Lett. **149B**, 311 (1984).
[53] E. van Lenthe and E. Baerends, J. Chem. Phys. **112**, 8279 (2000).
[54] S. Larsson, G. Leander, and I. Ragnarsson, Nucl. Phys. A **307**, 189 (1978).
[55] S. Ćwiok, J. Dudek, W. Nazarewicz, J. Skalski, and T. Werner, Comput. Phys. Commun. **46**, 379 (1987).
[56] L. Grodzins, Phys. Lett. **2**, 88 (1962).
[57] E. A. C. Lucken, *Nuclear Quadrupole Coupling Constants* (Academic Press, New York, 1969), p. 22.
[58] N. V. Zamfir, G. Hering, R. F. Casten, and P. Paul, Phys. Lett. B **357**, 515 (1995).